Optimal Terminals of a Multitransmitter Multireceiver Inductive Coupler With Equality Power Constraints

Rong He, *Member, IEEE*, Xinlin Wang, *Graduate Student Member, IEEE*, Haoyu Wang, *Senior Member, IEEE*, and Minfan Fu, *Senior Member, IEEE*

***Abstract*—This article develops a general and comprehensive ac analysis to study the optimal condition of a multitransmitter (TX) and multireceiver (RX) coupler. Based on the practical demands, a standard optimization problem is defined and solved by the Lagrange multiplier method. This article would analytically discuss the optimal coupler condition, discuss its physical meaning, and build a uniform perspective to understand representative systems. The meaning of the optimal analysis is justified by the evaluation and comparison of a circular pad-based coupler and a tripolar pad-based one. The influence of coupling and power distribution are effectively discussed based on the proposed ac analysis. The experiment builds a complete system to test the dc performance and justify the effectiveness of ac analysis. When the tripolar pad is used as the TX, a two-RX system would achieve 93.6% maximum dc efficiency with only 8.6% variation under all coupling conditions.**

***Index Terms*—Inductive power transfer (IPT), Lagrange multiplier method, multiple coils, optimal condition, power constraints.**

I. Introduction

INDUCTIVE power transfer (IPT) has found extensive application in the wireless charging of electronic devices. By utilizing a two-coil coupler, power can be transmitted from a transmitter (TX) to a receiver (RX) without physical cords. The coupler efficiency primarily depends on the coil quality factor and the coupling coefficient, and this feature guides the estimation of coupler ac efficiency [1], [2], [3], [4]. Besides, practical couplers must consider terminal constraints, such as driving current and load power, and then could be optimized to achieve system-level objectives [3], [5], [6]. The coupler characteristics provide a foundation for designing compensations to meet multiple demands [7], [8], [9], [10], [11], [12]. Through ac analysis, it is possible to achieve output regulation and maximum efficiency tracking, by controlling the inverters, rectifiers, and dc/dc converters [13], [14], [15], [16], [17], [18], [19]. Table I illustrates the importance of the basic coupler ac analysis in estimating efficiency, optimizing coupler, designing compensations, and controlling the system.

TABLE I
Current Works About ac Analysis

System	Terminal constraint	AC analysis	Coupler estimation	Coupler opti.	Comp. design	Active control
TX:1 RX:1	No	[20]	[1]	[2]	[7]	[20]
	Yes	[21]	[3]	[3]	[8]	[15]
TX:N_t RX:1	No	[22]	[1]	[1]	[12]	[22]
	Yes	[23]	/	[6]	[9]	[23]
TX:1 RX:N_r	No	[24]	[4]	[25]	[10]	[16]
	Yes	[21]	[3]	[5]	[11]	[17]
TX:N_t RX:N_r	No	[26]	[4]	[27]	[12]	[18]
	Yes	This article	This article	/	/	[19]

Multiple coils have been employed to enhance coupling in the presence of misalignment or multiload scenarios. The complexity of ac analysis increases when incorporating multiple TXs or RXs [25], [27]. Without considering the terminal constraints, several IPT systems have been developed to justify the benefits of multiple coils, as depicted in Table I. In single-TX systems, the optimal load concept has been developed from a single-RX case [20] to a general multi-RX scenario [24]. In systems with multiple TXs and a single RX, the optimal excitation currents and load have been derived to maximize ac efficiency [22], [23]. A comprehensive study has been conducted for a general system with multiple TXs and RXs [26]. However, these analyses often overlook the practical power demands imposed by various RXs.

By considering the terminal constraints, such as varied power demands, the complexity of ac analysis would further increase [refer to Table I]. For example, similar to one-TX one-RX systems, the output regulation and optimal efficiency tracking can be achieved in a multi-TX one-RX system based on the ac analysis [23]. These systems typically involve two objectives (power and efficiency) and multiple control variables (TX excitation currents and equivalent ac load), making the required ac analysis

Manuscript received 30 March 2023; revised 16 June 2023 and 14 July 2023; accepted 22 July 2023. Date of publication 31 July 2023; date of current version 1 September 2023. This work was supported by National N S F of China under Grant 52007120. Recommended for publication by Associate Editor Fei Lu. *(Corresponding author: Minfan Fu.)*

Rong He and Xinlin Wang are with the ShanghaiTech University, Shanghai 201210, China, also with the Shanghai Advanced Research Institute, Chinese Academy of Science, Shanghai 201210, China, and also with the University of Chinese Academy of Sciences, Beijing 100049, China (e-mail: herong@shanghaitech.edu.cn; wangxl3@shanghaitech.edu.cn).

Haoyu Wang and Minfan Fu are with the School of Information Science and Technology, ShanghaiTech University, Shanghai 201210, China, and also with the Shanghai Engineering Research Center of Energy Efficient and Custom AI IC, Shanghai 200040, China (e-mail: wanghy@shanghaitech.edu.cn; fumf@shanghaitech.edu.cn).

Color versions of one or more figures in this article are available at https://doi.org/10.1109/TPEL.2023.3299930.

Digital Object Identifier 10.1109/TPEL.2023.3299930

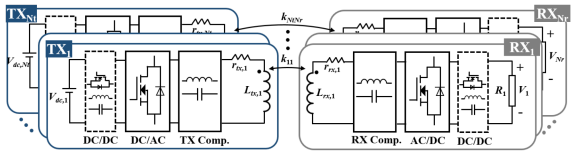

Fig. 1. General multi-TX multi-RX IPT system.

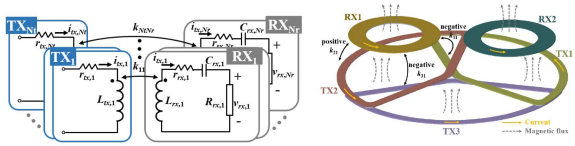

(a) (b)

Fig. 2. Coupler model. (a) AC model of a multi-TX multi-RX coupler. (b) Example 3TX-2RX coupler.

relatively straightforward for guiding system control. However, when additional RXs are introduced, the ac analysis needs to account for power distribution and its impact on coupling performance. For instance, in a one-TX multi-RX system, the difference between optimal driving and optimal loading schemes has been discussed in [21]. It is of significance to conduct a comprehensive study on the effects of driving and loading in a general multi-TX multi-RX system.

This article focuses on analyzing the ac behavior of the coupler, deriving the optimal condition, and discussing the effects of coupling and loading in a general multi-TX multi-RX system (see Table I). The practical power requirements are represented as equality constraints, while the ac terminal currents or loads are considered as control variables. This ac analysis can be defined as a standard optimization problem and solved using the Lagrange multiplier method [28]. A coupler without any power constraints is used as a reference for analyzing the global optimal condition in a similar manner. The conclusions drawn from this analysis have clear physical significance and greatly simplify the comparison of different representative couplers. To validate the effectiveness of the ac analysis, two types of couplers are evaluated and compared. In an experiment, the same example coupler is utilized to construct a fully functional dc system, incorporating compensation, an inverter, and a rectifier. The proposed ac analysis enables a qualitative prediction of the dc efficiency and assists in evaluating the coupler's performance prior to fabrication.

II. Coupler Analysis With Power Constraints

A. General System Configuration

Fig. 1 shows a general multi-TX multi-RX IPT system, which has N_t TXs and N_r RXs. For each TX, it at least includes a dc power source, an inverter, a TX compensation, and a TX coil. Meanwhile, an RX coil, an RX compensation, and a rectifier are necessary for a single RX. At the dc input and output terminals, additional dc/dc stages may be inserted for regulation purposes, such as input voltage modulation, TX-coil current modulation, output voltage modulation, and maximum efficiency tracking. In various controllable systems, although the direct control variables and the activation circuits are different, the final equivalent control effect is to modify the ac terminal conditions of the coupler, such as the ac driving current of the TX coil and the ac equivalent load resistance after the RX coil. Therefore, the ac characteristics of the multi-TX multi-RX resonant tank serve as the fundamentals of system-level analysis and control.

For example, it is well known that a maximum ac efficiency exists for a simple two-coil system, and this value is the natural feature of coupler. This maximum efficiency is used to estimate the coupling efficiency before any real dc tests. Meanwhile, based on the ac analysis, with fixed coil, operating frequency and coupling condition, the maximum coupler efficiency is achieved by an optimal load resistance, which is tracked by the active converters. If output voltage or current regulation is required, more controllable circuits are introduced in many prior papers [14], [15]. This article is devoted to a general ac analysis for multi-TX multi-RX coupler, based on which the existing IPT techniques (mostly demonstrated in a simplest system) could be extended for a multi-TX multi-RX scenario.

The maximum coupler efficiency should be a natural feature. In a series compensated IPT system, the coupler's maximum efficiency is determined by the coil quality factor and coupling coefficient, and does not depend on the compensation (assuming the additional components are ideal). Actually, the compensation just helps to reflect a pure resistor to the TX side. Using series compensation, the passive part of Fig. 1 is extracted as shown in Fig. 2(a). For TX_i, $i_{tx,i}$, $L_{tx,i}$, and $r_{tx,i}$ are the driving current, self-inductance, and equivalent series resistance (ESR) of the coil. For RX_j, $L_{rx,j}$ is the coil inductance, $r_{rx,j}$ is the coil ESR, $C_{rx,j}$ is the compensation capacitor and designed by $\omega L_{rx,j} - 1/(\omega C_{rx,j}) = 0$, $R_{rx,j}$ is the ac load, $i_{rx,j}$ is the coil current, and $v_{rx,j}$ is the ac output voltage. The mutual inductance between TX_i and RX_j is M_{ij}, and the coupling coefficient is $k_{ij} = M_{ij}/\sqrt{L_{tx,i}L_{rx,j}}$.

In a system with multiple TXs and RXs, the TX-RX coupling is utilized for power delivery. However, the TX-TX or RX-RX cross coupling (between the same-side coils) can result in an undesired energy circulation. To address this issue, practical systems employ coil decoupling techniques. For instance, TX coils can be strategically placed in an overlapping or orthogonal manner to cancel out cross coupling [29], [30], [31], [32]. RX coils can maintain sufficient clearance or incorporate shielding structures to minimize cross coupling effects [33], [34], [35]. Fig. 2(b) illustrates an example of a 3TX-2RX coupler, where the tripolar pad (TPP)-based TX is used to charge two RXs. In such multi-TX multi-RX systems, a reference is required to define the coupling, and bipolar mutual inductance, either positive or negative. Assuming all coils are wound in the same manner, when an anticlockwise current is injected into each coil, the direction of the TX-induced flux in the RX-coil plane determines the polarity of the mutual inductance. If the TX-induced flux has the same direction as the RX-induced flux, a positive mutual inductance with a positive coupling coefficient is defined. Conversely, if the flux directions are opposite, a negative coupling is considered. For example, when the yellow RX1 is positioned directly above

TX2 in Fig. 2(b), the right-hand rule suggests a positive coupling between TX2 and RX1, while a negative coupling is indicated between TX1 and RX1.

At the fundamental frequency, the ac model would use the basic phasor analysis to derive the ac characteristics. All the time-variant state variables could be represented by the phasor form. For example, the input excitation $i_{tx,i}$ is denoted as $\boldsymbol{I_{tx,i}}$, and its magnitude is $I_{tx,i}$. When the current of $\boldsymbol{I_{tx,1}}$ is assigned to be positive, the currents of the other TXs could be either positive or negative. The phase difference is not included in this article. The state equations for the RX-side circuit are

$$\sum_{i=1}^{N_t} j\omega M_{ij}\boldsymbol{I_{tx,i}} - (R_{rx,j}+r_{rx,j})\,\boldsymbol{I_{rx,j}} = 0, j \in [1, N_r] \quad (1)$$

where $\omega = 2\pi f$ is the angular frequency. The RX$_j$'s output power and the overall output power are

$$P_j = I_{rx,j}^2 R_{rx,j} \quad (2)$$

$$P = \sum_{j=1}^{N_r} P_j. \quad (3)$$

The loss of each TX and each RX are

$$P_{\text{loss,tx},i} = I_{tx,i}^2 r_{tx,i} \quad (4)$$

$$P_{\text{loss,rx},j} = I_{rx,j}^2 r_{rx,j}. \quad (5)$$

Thus, the ac efficiency of the coupler is

$$\eta_{\text{ac}} = P \Big/ \left(\sum_{i=1}^{N_t} P_{\text{loss,tx},i} + \sum_{j=1}^{N_r} P_{\text{loss,rx},j} + P \right). \quad (6)$$

This article tries to derive the optimal ac condition under practical constraints for a controllable system.

B. Efficiency Optimization

A practical RX would have a specific power requirement and its mutual inductance to all TXs. The RX-side active circuit may extract the required power based on its loading condition. For example, in a two-coil *LCC*-S IPT system, the output voltage is clamped by the input excitation current, and the equivalent ac resistance may be tuned by the dc–dc converter of RX side to absorb the target power. For a multi-RX scenario, each RX would have a power demand, and be defined as P_j. Each power demand defines an equality constraint for the tank, and combining (1) and (2) gives

$$P_j = \left| \left(\sum_{i=1}^{N_t} j\omega M_{ij}\boldsymbol{I_{tx,i}} \right) \Big/ (R_{rx,j}+r_{rx,j}) \right|^2 R_{rx,j}, j \in [1, N_r]. \quad (7)$$

There are total N_r power constraints. The maximization of η_{ac} becomes a standard optimization problem: its cost function is the overall loss [refer to (4) and (5)], its equality constraints are given in (7), and the variables are the TX excitation currents and RX current, i.e., $I_{tx,i}$ and $I_{rx,i}$. The standard form of above optimization problem is

$$\begin{aligned} \underset{I_{tx,i}, I_{rx,j}}{\text{minimize}} \quad & \sum_{i=1}^{N_t} I_{tx,i}^2 r_{tx,i} + \sum_{j=1}^{N_r} I_{rx,j}^2 r_j \\ \text{subject to} \quad & \left(\sum_{i=1}^{N_t} \omega M_{ij} I_{tx,i} \right) I_{rx,j} - P_j = 0, j \in [1, N_r]. \end{aligned} \quad (8)$$

This optimization problem would be solved by the Lagrange multiplier method, which is attractive for optimization under equality constraints [28]. Assuming $R_{rx,j} \gg r_{rx,j}$, the corresponding Lagrange function is given in the following:

$$\begin{aligned} L_P = & \sum_{i=1}^{N_t} I_{tx,i}^2 r_{tx,i} + \sum_{j=1}^{N_r} I_{rx,j}^2 r_{rx,j} \\ & + \sum_{j=1}^{N_r} \lambda_{P,j} \left(\left(\sum_{i=1}^{N_t} \omega M_{ij} I_{tx,i} \right) I_{rx,j} - P_j \right) \end{aligned} \quad (9)$$

where $\lambda_{P,j}$ is the Lagrange multiplier. The Lagrange function and the Lagrange multiplier do not have strong psychical meaning, and they are defined to solve a general optimization problem under equality constraint. In order to derive the optimal condition, it has to solve the following derivative equations simultaneously:

$$\partial L_P/\partial I_{tx,i} = \partial L_P/\partial I_{rx,j} = \partial L_P/\partial \lambda_{P,j} = 0. \quad (10)$$

When the above optimization problem is defined in a standard math form, abundant numerical optimization methods would help solve the optimal condition once the tank parameters are given. Therefore, the key contribution of this article is not to justify the existence of a solution or obtain the optimal solution when sufficient parameters are given. Instead, it tries to analytically explore an explicit circuit status with clear physical meaning, which would benefit the understanding of the mechanism of the optimal condition. Such kind of ac analysis is able to evaluate the coupling performance before a real test and then help guide the design of overall system.

Under the optimal condition, i.e., solving (10), the optimal TX current, RX current, and Lagrange multiplier would meet the following constraints:

$$I_{tx,i,P,\text{opt}} = \frac{1}{r_{tx,i}} \sum_{j=1}^{N_r} \omega M_{ij} \left(-\frac{\lambda_{P,j}}{2} \right)^{\frac{3}{2}} \sqrt{\frac{P_j}{r_{rx,j}}} \quad (11)$$

$$I_{rx,j,P,\text{opt}} = (-\lambda_{P,j}/2) \sqrt{P_j/r_{rx,j}} \quad (12)$$

$$\begin{aligned} & \left(-\frac{\lambda_{P,j}}{2} \right)^{\frac{1}{2}} \left\{ \sum_{i=1}^{N_t} \frac{\omega M_{ij}}{r_{tx,i}} \sum_{j=1}^{N_r} \omega M_{ij} P_j^{\frac{1}{2}} r_{rx,j}^{-\frac{1}{2}} \left(-\frac{\lambda_{P,j}}{2} \right)^{\frac{3}{2}} \right\} \\ & = P_j^{\frac{1}{2}} r_{rx,j}^{\frac{1}{2}}. \end{aligned} \quad (13)$$

In (11) and (12), it is clear that all the optimal currents are dependent on $\lambda_{P,j}$, which needs to solve (13).

Although $\lambda_{P,j}$ cannot be directly solved for a general case (numerical solutions are easily obtained from pure math point

TABLE II
OPTIMAL CONDITION FOR THREE SPECIAL SYSTEMS WITH POWER CONSTRAINTS

Coil number	Lagrange multiplier $\lambda_{P,j}$	Opt.current $I_{tx,i,P,opt}$	Opt. load $R_{\mathrm{rx},j,P,\mathrm{opt}}$	AC efficiency $\eta_{ac,P,opt}$
Case A: $N_t = 1, N_r = 1$	$-\frac{2\sqrt{r_{\mathrm{tx},1} r_{\mathrm{rx},1}}}{\omega M_{11}}$	$\left(\frac{1}{r_{\mathrm{tx},1}} \frac{P^2 r_{\mathrm{rx},1}}{\omega^2 {M_{11}}^2}\right)^{\frac{1}{4}}$	$r_{\mathrm{rx},1}\sqrt{\frac{\omega^2 {M_{11}}^2}{r_{\mathrm{tx},1} r_{\mathrm{rx},1}}}$	$\frac{\sqrt{\frac{\omega^2 {M_{11}}^2}{r_{\mathrm{tx},1} r_{\mathrm{rx},1}}}-1}{\sqrt{\frac{\omega^2 {M_{11}}^2}{r_{\mathrm{tx},1} r_{\mathrm{rx},1}}}+1}$
Case B: $N_t > 1, N_r = 1$	$-2r_{\mathrm{rx},1}^{\frac{1}{2}}\left(\sum_{i=1}^{N_t}\frac{\omega^2 M_{i1}^2}{r_{\mathrm{tx},i}}\right)^{-\frac{1}{2}}$	$\frac{\omega M_{i1}}{r_{\mathrm{tx},i}}\left(\frac{{P_1}^2 r_{\mathrm{rx},1}}{\left(\sum_{i=1}^{N_t}\frac{\omega^2 M_{i1}^2}{r_{\mathrm{tx},i}}\right)^3}\right)^{\frac{1}{4}}$	$r_{\mathrm{rx},1}\sqrt{\sum_{i=1}^{N_t}\frac{\omega^2 M_{i1}^2}{r_{\mathrm{tx},i} r_{\mathrm{rx},1}}}$	$\frac{\sqrt{\sum_{i=1}^{N_t}\frac{\omega^2 M_{i1}^2}{r_{\mathrm{tx},i} r_{\mathrm{rx},1}}}-1}{\sqrt{\sum_{i=1}^{N_t}\frac{\omega^2 M_{i1}^2}{r_{\mathrm{tx},i} r_{\mathrm{rx},1}}}+1}$
Case C: $N_t = 1, N_r > 1$	$\frac{-2r_{\mathrm{rx},j}P_j}{\omega^2 M_{1j}^2}\left(\frac{1}{r_{\mathrm{tx},1}}\sum_{j=1}^{N_r}\frac{P_j^2 r_{\mathrm{rx},j}}{\omega^2 M_{1j}^2}\right)^{-\frac{1}{2}}$	$\left(\frac{1}{r_{\mathrm{tx},1}}\sum_{j=1}^{N_r}\frac{P_j^2 r_{\mathrm{rx},j}}{\omega^2 M_{1j}^2}\right)^{\frac{1}{4}}$	$\frac{\omega^2 M_{1j}^2}{P_j}\left(\frac{1}{r_{\mathrm{tx},1}}\sum_{j=1}^{N_r}\frac{P_j^2 r_{\mathrm{rx},j}}{\omega^2 M_{1j}^2}\right)^{\frac{1}{2}}$	$\frac{\sum_{j=1}^{N_r} P_j}{\sum_{j=1}^{N_r} P_j + 2\left(r_{\mathrm{tx},1}\sum_{j=1}^{N_r}\frac{P_j^2 r_{\mathrm{rx},j}}{\omega^2 M_{1j}^2}\right)^{\frac{1}{2}}}$

of view), there are some interesting findings based on the above derivations. Taking (11) and (12) into the overall losses of TX and RX [refer to (4) and (5)], it shows that the optimal condition would indicate a loss balance situation, i.e.

$$\sum_{i=1}^{N_t} P_{\mathrm{loss,tx},i} = \sum_{j=1}^{N_r} P_{\mathrm{loss,tx},j} = -\sum_{j=1}^{N_r} \lambda_{P,j} P_j/2. \tag{14}$$

This finding has been proved in a one-TX one-RX system. This conclusion can be used to evaluate the deviation of a practical condition from its theoretical status.

Since the analytical solution of optimal condition is mainly determined by the $\lambda_{P,j}$, this article would further explore the theoretical boundary when an analytical solution of $\lambda_{P,j}$ exists. The number of TX or RX can be defined to generate several special cases. For example, Case A means $N_t = 1, N_r = 1$ (i.e., one-TX one-RX), Case B means $N_t > 1, N_r = 1$ (i.e., multi-TX one-RX), Case C means $N_t = 1, N_r > 1$ (i.e., one-TX multi-RX), and Case D means $N_t > 1, N_r > 1$ (i.e., multi-TX multi-RX). For the first three cases (A–C), the Lagrange multipliers can be derived directly, which are given in the second column of Table II. All the other state variables are solved based on $\lambda_{P,j}$ and given in the table. For Case D, (13) becomes a polynomial equation, which could not be solved by simple rooting finding formula. Another two subcases need to be defined for further discussion: Case D1($N_r = 2$) and Case D2 ($N_r > 2$). In the appendix, it is proved that Case D1 would be the boundary that an analytical solution exists. When $N_r > 2$, the numerical methods have to be used to calculate the maximum efficiency based on the same optimization problem.

Having explicit solutions for Cases A–C would be beneficial in understanding the physical implications of the optimal condition. In Table II, many state variables are dependent on coupling under optimal conditions. However, there are instances where certain cases demonstrate power independence. For instance, when $N_r = 1$, the Lagrange multiplier becomes power independent, resulting in power-independent values for $R_{rx,j,P,\mathrm{opt}}$ and $\eta_{\mathrm{ac},P,\mathrm{opt}}$. From a control perspective, this implies that the optimal load can be achieved through the RX-side circuits, allowing the TX-side currents to meet the power demand. This enables separate regulation of power and efficiency. This reason has been validated in both single-TX and multi-TX systems [23]. Due to space limitations, this article will not explore all the possibilities for system design and control, focusing instead on the accuracy and effectiveness of the derived ac characteristics.

III. COUPLER ANALYSIS WITHOUT POWER CONSTRAINTS

A. Efficiency Optimization

When a multi-TX multi-RX coupler is used without any constraints, an optimal efficiency also exists and is defined as the global maximum efficiency ($\eta_{\mathrm{ac,opt}}$). It means all the ac terminal state variables are used to maximize this efficiency. For example, in the well-known two-coil system, $\eta_{\mathrm{ac,opt}}$ is proportional to the coupling coefficient and coil quality factor, but independent of the power. This section would devote to the coupler maximum efficiency without power demands. Such an optimal condition has been reported in [26]. However, the derived results are not straightforward and lack of sufficient practical meaning. This article is devoted to building a general understanding of a multi-TX multi-RX coupler and then discussing the influence of power constraints.

When it comes to a multi-TX multi-RX scenario, the defined optimization in previous section cannot be simplified by removing the equality power constraints. It needs to use the original state equation as the equality constraint. The standard optimization problem is defined as

$$\begin{aligned} \underset{I_{tx,i},I_{rx,j}}{\text{minimize}} \quad & \frac{\sum_{j=1}^{N_r} I_{rx,j}^2 R_{rx,j}}{\sum_{i=1}^{N_t} I_{tx,i}^2 r_{tx,i} + \sum_{j=1}^{N_r} I_{rx,j}^2 \left(R_{rx,j} + r_{rx,j}\right)} \\ \text{subject to} \quad & \sum_{i=1}^{N_t} \omega M_{ij} I_{tx,i} = I_{rx,j}\left(R_{rx,j} + r_{rx,j}\right), j \in [1, N_r]. \end{aligned} \tag{15}$$

Assuming λ_j is a Lagrange multiplier, the new Lagrange function could be written as

$$\begin{aligned} L = & \frac{\sum_{j=1}^{N_r} I_{rx,j}^2 R_{rx,j}}{\sum_{i=1}^{N_t} I_{tx,i}^2 r_{tx,i} + \sum_{j=1}^{N_r} I_{rx,j}^2 r_{rx,j} + \sum_{j=1}^{N_r} I_{rx,j}^2 R_{\mathrm{rax},j}} \\ & + \sum_{j=1}^{N_r} \lambda_j \left(\sum_{i=1}^{N_t} \omega M_{ij} I_{tx,i} - \left(R_{rx,j} + r_{rx,j}\right) I_{rx,j}\right) \end{aligned} \tag{16}$$

where the first fractional term means the cost function [i.e., the ac efficiency of (6)], and the second term is the equality constraint

TABLE III
OPTIMAL CONDITION FOR THREE SPECIAL SYSTEM WITHOUT POWER CONSTRAINTS

Coil number	β	Opt. current $I_{\text{tx},i,\text{opt}}$	Opt. load $R_{\text{rx},j,\text{opt}}$	AC efficiency $\eta_{\text{ac,opt}}$
Case A: $N_t = 1, N_r = 1$	$\sqrt{\frac{\omega^2 M_{11}^2}{r_{\text{tx},1} r_{\text{rx},1}}}$	$I(P)$	$r_{\text{rx},1}\sqrt{\frac{\omega^2 M_{11}^2}{r_{\text{tx},1} r_{\text{rx},1}}}$	$\left(\sqrt{\frac{\omega^2 M_{11}^2}{r_{\text{tx},1} r_{\text{rx},1}}} - 1\right) / \left(\sqrt{\frac{\omega^2 M_{11}^2}{r_{\text{tx},1} r_{\text{rx},1}}} + 1\right)$
Case B: $N_t > 1, N_r = 1$	$\sqrt{\sum_{i=1}^{N_t} \frac{\omega^2 M_{i1}^2}{r_{\text{tx},i} r_{\text{rx},1}}}$	$\frac{M_{i1}}{r_{\text{tx},i}} I(P)$	$r_{\text{rx},1}\sqrt{\sum_{i=1}^{N_t} \frac{\omega^2 M_{i1}^2}{r_{\text{tx},i} r_{\text{rx},1}}}$	$\left(\sqrt{\sum_{i=1}^{N_t} \frac{\omega^2 M_{i1}^2}{r_{\text{tx},i} r_{\text{rx},1}}} - 1\right) / \left(\sqrt{\sum_{i=1}^{N_t} \frac{\omega^2 M_{i1}^2}{r_{\text{tx},i} r_{\text{rx},1}}} + 1\right)$
Case C: $N_t = 1, N_r > 1$	$\sqrt{\sum_{j=1}^{N_r} \frac{\omega^2 M_{1j}^2}{r_{\text{tx},1} r_{\text{rx},j}}}$	$I(P)$	$r_{\text{rx},j}\sqrt{\sum_{j=1}^{N_r} \frac{\omega^2 M_{1j}^2}{r_{\text{tx},1} r_{\text{rx},j}}}$	$\left(\sqrt{\sum_{j=1}^{N_r} \frac{\omega^2 M_{1j}^2}{r_{\text{tx},1} r_{\text{rx},j}}} - 1\right) / \left(\sqrt{\sum_{j=1}^{N_r} \frac{\omega^2 M_{1j}^2}{r_{\text{tx},1} r_{\text{rx},j}}} + 1\right)$

defined by (1). This way, the Lagrange multiplier method is still effective.

The optimal condition still needs to solve the following derivative equations:

$$\partial L/\partial I_{tx,i} = \partial L/\partial I_{rx,j} = \partial L/\partial R_{rx,j} = \partial L/\partial \lambda_j = 0. \quad (17)$$

The final solutions are solved as

$$R_{rx,j,\text{opt}}/r_{rx,j} = \beta \quad (18)$$

$$\frac{1}{I_{tx,i,\text{opt}} r_{tx,i}} \sum_{j=1}^{N_r} \frac{\omega M_{ij}}{r_{rx,j}} \sum_{i=1}^{N_t} \omega M_{ij} I_{tx,i,\text{opt}} = \beta^2 - 1 \quad (19)$$

where the physical meaning of β is the resistance ratio under optimal value. From math point of view, the function of β is similar to that of $\lambda_{P,j}$ in (13), i.e., whether an explicit β exists determines the existence of explicit form of all the other state variables. Given β, the global maximum efficiency is

$$\eta_{\text{ac,opt}} = (\beta - 1)/(\beta + 1). \quad (20)$$

Although the maximum ac efficiency is derived based on the resistance ratio β, it should be noted that the optimal terminal resistance are determined by the coupler states, i.e., the parameters and the coupling. Similar to the coupler with power constraints, the optimal conditions for Cases A–C can be analytically solved by (18)–(20) directly. All of results are listed in Table III, where optimal current $I(P)$ is decided by output power. When the coupler maximize its efficiency, there is one freedom $I(P)$ left, which can be an arbitrary value. Therefore, $I(P)$ is a function of the overall power level. For Case D, the explicit form does not exist.

B. Influence of Power Constraints

The optimal characteristics of a coupler, in the absence of power constraints, accurately reflect its inherent properties. For instance, it is widely recognized that the efficiency ($\eta_{\text{ac,opt}}$) of a one-TX one-RX coupler is influenced by factors, such as coil ESR and mutual coupling. However, the introduction of power constraints implies that the optimal coupler characteristics become dependent on power level. Consequently, the efficiency drop caused by power constraints serves as a valuable tool for designers to assess the practical utilization of a coupler. The ideal performance of a coupler, represented by $\eta_{\text{ac,opt}}$, aids in determining whether the existing coupling conditions can guarantee sufficient efficiency. On the other hand, $\eta_{\text{ac},P,\text{opt}}$ is employed to evaluate the practical performance of the coupler when power demands are satisfied. Therefore, the efficiency drop ($\Delta\eta_{\text{ac}} = \eta_{\text{ac,opt}} - \eta_{\text{ac},P,\text{opt}}$) plays a critical role in assessing the tradeoffs made by the coupler in real-world scenarios.

The impact of power constraints can be analyzed by comparing the information presented in Tables II and III. In Case A, both tables demonstrate that the optimal load and efficiency remain independent of power. In addition, the values of $R_{rx,j,P,\text{opt}}$ and $R_{rx,j,\text{opt}}$ are equivalent, as well as $\eta_{\text{ac},P,\text{opt}}$ and $\eta_{\text{ac,opt}}$, resulting in $\Delta\eta_{\text{ac}} = 0$. Consequently, in Table III, $I_{tx,i,\text{opt}}$ can be assumed to any value, which corresponds to the specific power demand in Table II. Moving to Case B, it shows that $R_{rx,j,P,\text{opt}}$ and $R_{rx,j,\text{opt}}$ remain unchanged, as well as $\eta_{\text{ac},P,\text{opt}}$ and $\eta_{\text{ac,opt}}$, resulting in $\Delta\eta_{\text{ac}} = 0$. However, when multiple TX coils are involved, the TX currents need to be modulated to concentrate toward a single RX. This is expressed as $I_{tx,i,\text{opt}} = I(P)\frac{M_{i1}}{r_{tx,i}}$ in Table III, which implies

$$(I_{tx,1} r_{tx,1})/M_{11} = (I_{tx,2} r_{tx,2})/M_{21} = \cdots = (I_{tx,N_t} r_{tx,N_t})/M_{N_t 1}. \quad (21)$$

Despite the existence of N_t TX currents for efficiency optimization, $(N_t - 1)$ control variables are utilized to satisfy the constraints mentioned in (21). Only one current magnitude, denoted as $I(P)$, remains for power regulation. In the case of a single RX, this solitary control variable proves to be satisfactory for meeting the load demand without compromising the efficiency of the coupler, denoted as $\Delta\eta_{\text{ac}} = 0$. However, in scenarios involving multiple RXs, such as Case C, both $R_{rx,j,P,\text{opt}}$ ($\neq R_{rx,j,\text{opt}}$) and $\eta_{\text{ac},P,\text{opt}}$ ($\neq \eta_{\text{ac,opt}}$) become dependent on power as indicated in Table II. To achieve the maximum global efficiency while maximizing the coupler efficiency, relying solely on the single TX current is inadequate given the power restrictions, resulting in $\Delta\eta_{\text{ac}} > 0$.

IV. COUPLER ESTIMATION

A. Example Setup

The basic ac characteristics of a coupler serve as the fundamental of coupler evaluation, coupler optimization, and system design and control. Prior works have broadly reported such kinds of achievements, especially for the simplest one-TX one-RX case. This article would use a coupler evaluation problem to justify the accuracy of the derivation and meaning of the ac analysis. In practice, the target RX and charging area would be defined, and then a customized TX should be proposed to meet the requirements. Therefore, a two-RX application is

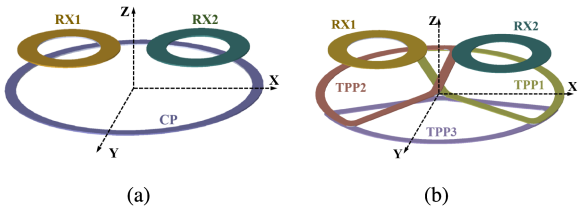

Fig. 3. Different 2-RX couplers. (a) Coupler 1: Using circular pad (CP) as TX. (b) Coupler 2: Using TPP as TX.

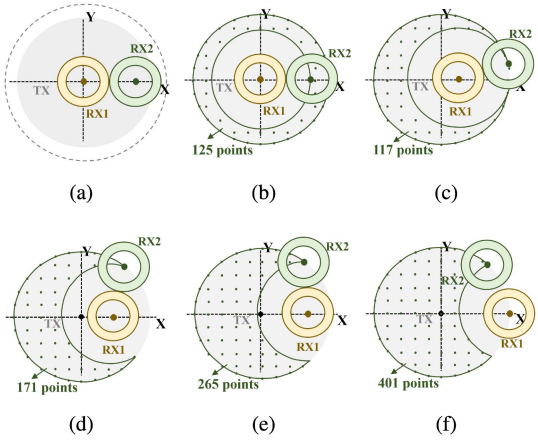

Fig. 4. Simulation setup. (a) Top view. (b) RX1 at (0 mm, 0 mm). (c) RX1 at (0 mm, 50 mm). (d) RX1 at (0 mm, 100 mm). (e) RX1 at (0 mm, 150 mm). (f) RX1 at (0 mm, 200 mm).

TABLE IV
COUPLER PARAMETERS

	CP	TPP1	TPP2	TPP3	RX1	RX2
L_{tx} or L_{rx} (μH)	92.0	53.5	52.7	53.6	59.1	59.1
r_{tx} or r_{rx} (Ω)	0.26	0.24	0.25	0.24	0.20	0.20

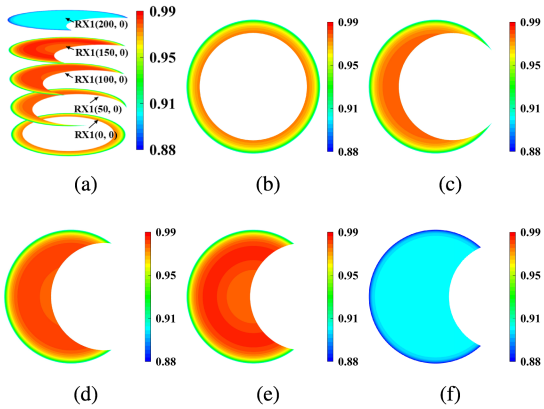

Fig. 5. $\eta_{\text{ac},P,\text{opt}}$ of CP-based coupler under coupling variation. (a) Overall. (b) RX1 at (0 mm, 0 mm). (c) RX1 at (0 mm, 50 mm). (d) RX1 at (0 mm, 100 mm). (e) RX1 at (0 mm, 150 mm). (f) RX1 at (0 mm, 200 mm).

defined, and the problem is to evaluate the TX solution when the moving freedom is given. As shown in Fig. 3, two RXs are allowed to move within a circular area above the TX. There are two candidate solutions: Coupler 1 would use a CP as TX and Coupler 2 would use a TPP. The proposed ac analysis could quickly compare the coupler performance under practical demand without a real-system test. Several interesting and general conclusions can be drawn through this case study.

The proposed ac analysis needs the coupler parameters, coupling conditions, and power demands for efficiency calculation. Within a wide range of moving areas, all the coupler parameters are extracted from the finite-element-analysis simulations to ensure high accuracy for the postestimation. Since the RXs are allowed to freely move within a given area, this article needs to build a uniform coordinate to indicate the coupling variation. As shown in Fig. 4(a) (a top view), the TX coil is defined by the gray solid circle. When the center of RXs does not move outside the TX-coil area, the maximum charging area is defined by the dotted circle. Different coupling conditions are discussed in Fig. 4(b)–(e). In Fig. 4(b), RX1 is fixed at the center. The vertical distance between TX and RX is divided into two conditions (i.e., 5 and 80 mm). When there is no overlapping between two RXs, the center of RX2 will move within the dotted area. When the RX1 is located at (0 mm, 50 mm), it would give a dotted area for RX2's center, as shown in Fig. 4(c). As RX1 gradually touches the charging area boundary, the dotted area would gradually change in Fig. 4(c)–(f), which is similar to the sun shape during an eclipse process. In Fig. 4(b)–(f), the sample points are evenly placed within the dotted area, and each point represents a specific RX placement and defines a coupling condition. There are a total of 1079 points or coupling conditions to be evaluated.

B. Efficiency Estimation

The influence of vertical distance and power distribution is discussed with the help of ac analysis. The coupler is evaluated at 200 kHz, and all the coil parameters are given in Table IV. Initially, the vertical distance is set at 5 mm, and two different power distributions are studied, i.e., an even power distribution ($P_1 = P_2 = 20$ W) and an uneven power distribution ($P_1 = 3P_2 = 30$ W). Note that both systems would have the same overall power.

Under even power distribution, $\eta_{\text{ac},P,\text{opt}}$ of Coupler 1 (using CP) is calculated based on the previous ac analysis and shown in Fig. 5. Each RX position of Fig. 4(b) (i.e., an observation point) would have an efficiency data in Fig. 5(b). Therefore, the coupling variation defined by dotted area of Fig. 4(b)–(f) would lead to a same-shape colored efficiency map in Fig. 5(b)–(f). All these maps are shown in Fig. 5(a) for different RX1 positions. When the TPP-based TX is adopted, the efficiency for different coupling is shown in Fig. 6. The efficiency of most points are above 90%. When RX1 moves to the edge position of CP-based TX, the efficiency drop is clear as shown in Fig. 5(f). From the math point of view, by using more TX coils, the excitation currents of TPP-based TX are able to be tuned to overcome this issue as shown in Fig. 6(f). From the control point of view, selective activation of multiple coils and control over the excitation current magnitude provide increased flexibility in flux control. It is important to note, however, that having more TX coils does not necessarily guarantee higher efficiency for any coupling condition.

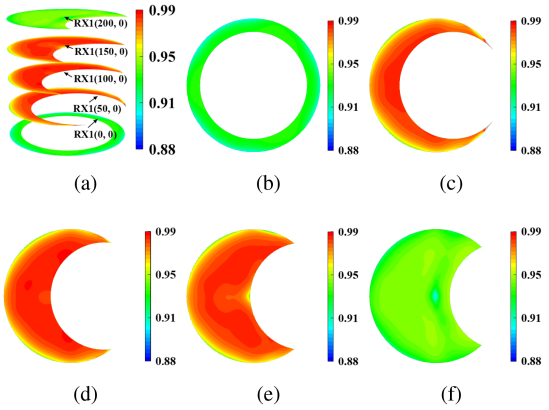

Fig. 6. $\eta_{\mathrm{ac},P,\mathrm{opt}}$ of TPP-based coupler under coupling variation. (a) Overall. (b) RX1 at (0 mm, 0 mm). (c) RX1 at (0 mm, 50 mm). (d) RX1 at (0 mm, 100 mm). (e) RX1 at (0 mm, 150 mm). (f) RX1 at (0 mm, 200 mm).

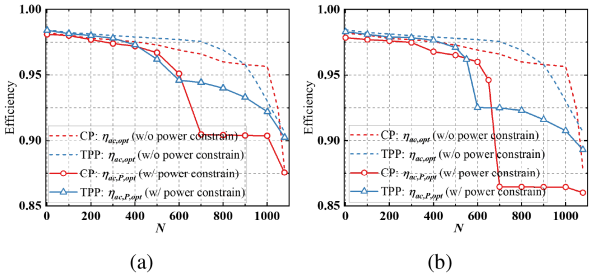

Fig. 7. AC efficiency estimation when $d = 5$ mm. (a) Even power distribution. (b) Uneven power distribution.

A direct observation of Figs. 5 and 6 is not straightforward to compare the efficiency under coupling variation. Refer to Fig. 4, there are a total of 1079 observation points (within five representative dot areas) to describe the varied RX placement. Therefore, all the efficiency data of the sample points are summarized in Fig. 7. The horizontal axis, denoted as N, represents the number of data points where the efficiency surpasses the corresponding value on the vertical axis. To illustrate, consider the red-circle line representing the CP-based system. The leftmost data point indicates $N = 1$ and $\eta_{\mathrm{ac}} = 98\%$, implying that there exists a single observation point where the efficiency exceeds 98%. Similarly, the rightmost data point represents $N = 1079$ and $\eta_{\mathrm{ac}} = 87.5\%$. This indicates that all 1079 data points exhibit an efficiency greater than 87.5%, with this particular efficiency value determined by the worst case scenario. It is evident that efficiency decreases as N increases. When the RXs are randomly positioned, and there is an uncertainty in the coupling, a higher curve for the coupler signifies a greater potential for higher efficiency.

When there is no power constraints, the red-dash curve would represent $\eta_{\mathrm{ac,opt}}$ for a CP-based system. The gap between the dash line and circle line ($\eta_{\mathrm{ac,opt}}$ and $\eta_{\mathrm{ac},P,\mathrm{opt}}$) reflects the sacrifice of coupler efficiency when meeting the power demands. When N is large, a large gap would occur. These sample points have a common feature, i.e., a large coupling coefficient difference between k_{11} and k_{12}. Under this scenario, a system with no power constraint would deliver more power to the RX with larger coupling for efficiency optimization. Once the power constraints are included, the coupler has to sacrifice its efficiency.

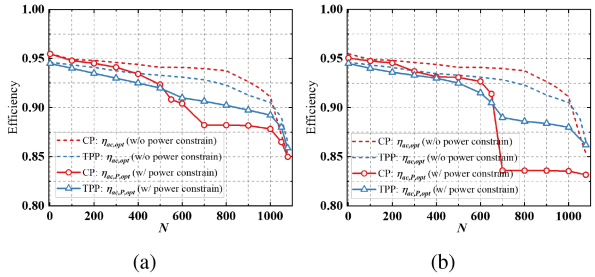

Fig. 8. AC efficiency estimation when $d = 80$ mm. (a) Even power distribution. (b) Uneven power distribution.

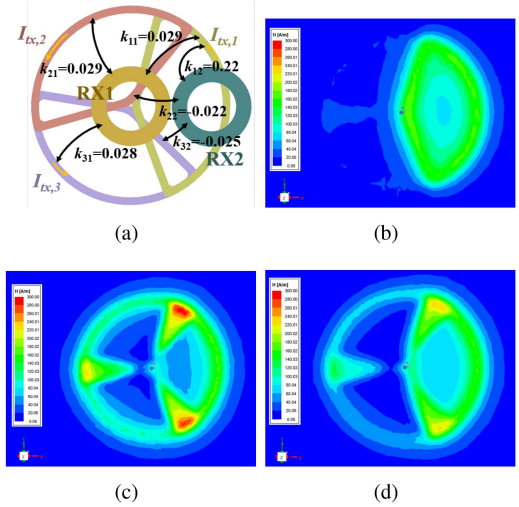

Fig. 9. Magnetic field intensity of TX when RX1 at (0 mm, 0 mm, 5 mm) and RX2 at (160 mm, 0 mm, 5 mm). (a) Setup. (b) Without power constraints. (c) $P_1 = P_2 = 20$ W. (d) $P_1 = 10$ W and $P_2 = 30$ W.

Besides the convenient evaluation of $\eta_{\mathrm{ac,opt}}$ and $\eta_{\mathrm{ac},P,\mathrm{opt}}$, the proposed ac analysis is very effective to compare $\eta_{\mathrm{ac},P,\mathrm{opt}}$ for various couplers. Fig. 7(a) compares $\eta_{\mathrm{ac},P,\mathrm{opt}}$ of TPP-based system and CP-based one at the selected sampling points. The TPP-based system has a higher global peak value ($N = 1$) and a smaller efficiency variation ($N \in [1, 1079]$). When uneven power distribution occurs, the conclusion does not change as shown in Fig. 7(b).

When the charging distance equals 80 mm, an another efficiency estimation is carried out. Detailed efficiency data could still be calculated and compared in Fig. 8. In terms of efficiency variation, the TPP-based system is still better. The selective excitation is helpful to maintain the efficiency when RXs are located at the edge position. When $N < 500$ in Fig. 8(a), $\eta_{\mathrm{ac},P,\mathrm{opt}}$ of CP-based system becomes better. This is because a larger single coil is more powerful to ensure sufficient flux when the distance is large. Similar conclusion is also valid for uneven power distribution in Fig. 8(b).

C. Magnetic Field Analysis

Coupling and power conditions determine optimal input excitation, and further affect the magnetic field. Two RXs are placed in an example position of Fig. 9(a), which also shows the coupling coefficients. Without the power constraints, the

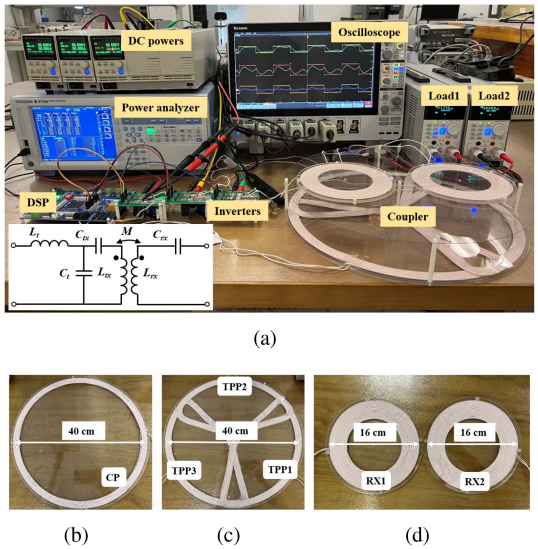

Fig. 10. Experiment setup. (a) System overview. (b) CP. (c) TPP. (d) Two RXs.

optimal currents are solved to generate the field of Fig. 9(b). Most of the power would be offered by TX1 because it has stronger coupling to both RXs compared with the other TXs. When the RXs have specific power demands, such as $P_1 = P_2 = 20$ W, the required optimal currents could still be derived and used for field excitation in Fig. 9(c). It means all the TXs are excited, and the current of TX1 is a little larger. For uneven power distribution, i.e., increasing P_2 to 30 W and decreasing P_1 to 10 W. Fig. 9(d) shows that the currents of TX2 and TX3 are decreased to meet the new power demands since both of them have negative coupling. There are two basic qualitative conclusions to ensure high efficiency. The TX coil with stronger coupling to RX should have higher excitation, and the TX coil far from the higher power RX should decrease its current. The proposed optimization helps give a quantitative estimation.

V. Experiment Verification

The final experimental setup is shown in Fig. 10(a). Every TX coil is compensated by *LCC* compensation and driven by a full bridge inverter. The TX coil current is only tuned by the input dc voltage. The RX coil would adopt the series compensation and is connected to a bridge rectifier. An electronic load would work at a constant power mode to mimic the real power demand. The overall output power is 40 W for two RXs. The layout of the coupler is shown in Fig. 10(b),–(d). Two RXs of Fig. 10(d) will be placed right above the TX as shown in Fig. 10(a). All these coils are fabricated by litz wire (AWG38, 0.1 mm × 150). The self-inductance and ESRs of these coils are measured by impedance analyzer. The above theoretical analysis is independent to operating frequency, which is chosen at 200 kHz in this experiment to benefit the coil quality factor. The other components are designed based on a *LCC*-S compensation. All values are given in Table V.

In the ac analysis, only the efficiency is evaluated for a multi-TX multi-RX coupler. The final test would include the inverter and the rectifier to have a dc/dc efficiency. Similar to the two-coil coupler, its ac characteristic is a determinant factor from the overall perspective. Its ac-level conclusion would be seen at the dc test. During the test, the input voltage of the inverter is manually tuned to adjust the TX coil current according to the calculated currents of the ac analysis. A typical waveform for the inverter output is given in Fig. 11. All the terminal information is provided, including the three input terminals and two output ones. When the input current i_{in1} is set as the reference, i_{in2} and i_{in3} are out of phase. Such a feature reflects the existence of bipolar mutual inductance.

The coupling variation condition of Fig. 4(e) would be used as an example to compare the difference between ac calculation and dc test. When vertical distance is 5 mm, the comparison for CP-based system is shown in Fig. 12. Fig. 12(a) shows the efficiency map when both RXs have the same output power, and Fig. 12(b) compares the efficiency under uneven power distribution. Both figures show that the proposed ac analysis is sufficient to evaluate the final dc results under coupling and loading variation. The active circuits will cause an efficiency drop due to the additional losses but will not affect the basic characteristics of the efficiency map. Similar comparison is given for a TPP-based two-RX system in Fig. 13. The conclusion is still valid. Comparing the dc efficiency of Figs. 12 and 13, it is also clear that more TX coils would be helpful for improving the efficiency and lowering the variation of efficiency under RX position change.

TABLE V
Parameters of Resonant Tanks

	CP	TPP1	TPP2	TPP3	RX1	RX2
Turns number	10	10	10	10	18	18
L_{tx} or L_{rx} (μH)	92.0	53.5	52.7	53.6	59.1	59.1
r_{tx} or r_{rx} (Ω)	0.26	0.24	0.25	0.24	0.20	0.20
L_t (μH)	24.9	18.64	14.58	18.2	/	/
C_t (nF)	25.42	33.97	43.42	34.79	/	/
C_{tx} (nF)	9.43	18.17	16.61	17.92	/	/
C_{rx} (nF)	/	/	/	/	10.72	10.72

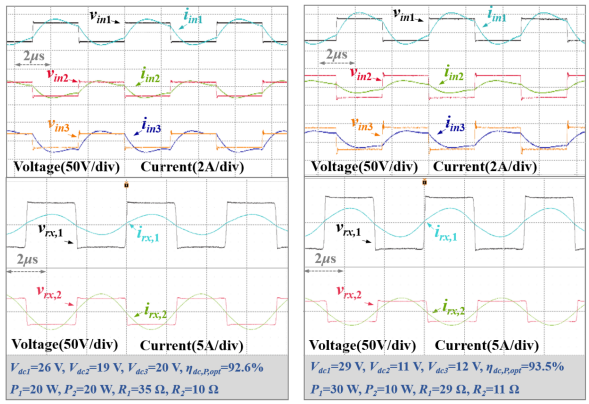

Fig. 11. Inverter output waveform and receiving coil waveform. v_{in}: The output voltage of the inverter. i_{in}: The output current of the inverter. (a) Even power distribution: $P_1 = P_2 = 20$ W (b) Uneven power distribution: $P_1 = 3P_2 = 30$ W.

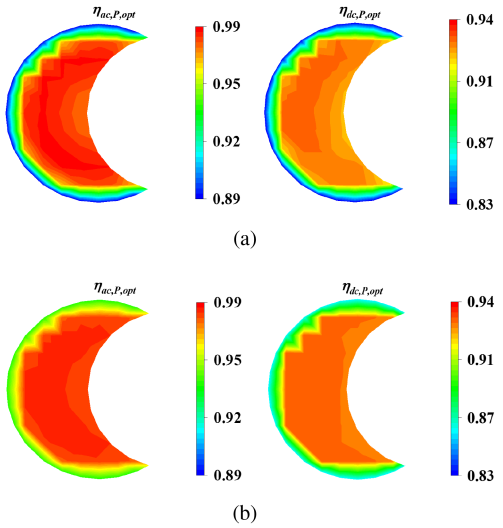

Fig. 12. AC and DC efficiency comparison of CP-based systems. (a) Even power distribution. (b) Uneven power distribution.

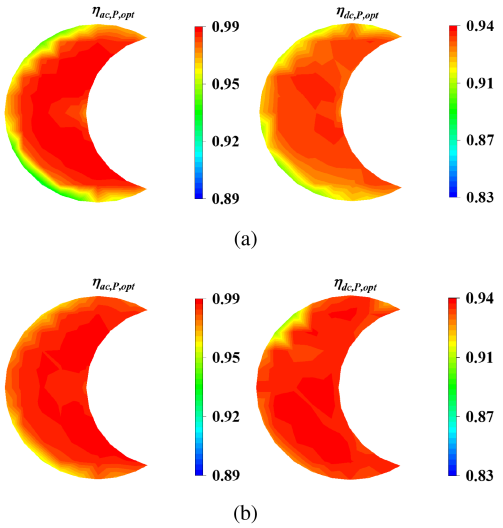

Fig. 13. AC and DC efficiency comparison of TPP-based systems. (a) Even power distribution. (b) Uneven power distribution.

When the RXs move, as shown in Fig. 4(b)–(f), all dc efficiencies are recorded and compared in Fig. 14. Here the ac efficiency is calculated like Fig. 7, but it is based on the real coupler parameters. For both CP-based system and TPP-based one, the original conclusion (drawn based on the ac analysis) is still valid, i.e., the TPP-based system is helpful to stabilize the efficiency. For example, under even power distribution, the peak $\eta_{\mathrm{dc},P,\mathrm{opt}}$ of TPP-based system is 93.6% when $N = 1$. For most coupling conditions, it is better than the efficiency of CP-based system. For either CP-based system or TPP-based one, the gap between $\eta_{\mathrm{ac},P,\mathrm{opt}}$ and $\eta_{\mathrm{dc},P,\mathrm{opt}}$ is caused by the active circuits. For both systems, Fig. 14 clearly shows the dc characteristics are determined by the ac ones. Therefore, the proposed ac analysis and coupler efficiency estimation could quickly tell the performance of a candidate coupler.

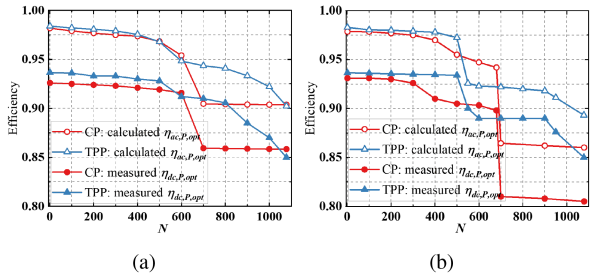

Fig. 14. AC and DC efficiency comparison for all sampling points. (a) Even power distribution. (b) Uneven power distribution.

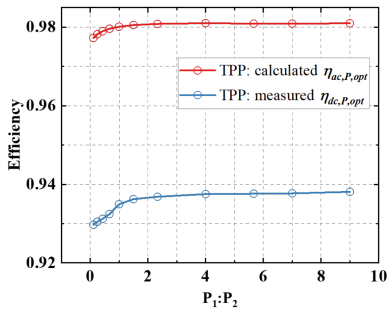

Fig. 15. AC and DC efficiency comparison for different output power ratios.

In the previous tests, only two loading conditions are measured for various systems, i.e., even and uneven power distribution. Since the ac calculation is valid for any power condition, the TPP-based system is further tested for a fixed position [RX1(150 mm, 0 mm), RX2(−80 mm, 0 mm)]. By fixing the overall output power at 40 W, different power ratios are measured and compared with the calculation results in Fig. 15. The proposed ac estimation could still predict the basic trends and the influence of the power distribution.

VI. Conclusion

A comprehensive ac analysis is proposed for the study and estimation of a coupler. By defining the practical power demands as equality constraints, a standard optimization problem is built and solved by the Lagrange multiplier method. The boundary of explicit solutions is discussed, and the practical meaning of the optimal conditions are explained referring to the well-known characteristics of a two-coil coupler. The coupler performance without any power constraints is also analyzed in a uniform manner, which helps discuss the influence of power demands. Based on the proposed ac analysis, a coupler estimation approach is proposed for a two-RX example application. It could quickly judge the efficiency variation under different loading and coupling conditions and guide the selections of TX. In the experiment, various couplers are fabricated and tested in complete dc systems. The consistency between the ac and dc efficiencies justifies the accuracy and effectiveness of the optimal ac analysis.

APPENDIX A

For Case D1: Assuming $x = -\frac{\lambda_{P,1}}{2}$ and $y = -\frac{\lambda_{P,2}}{2}$, it can be viewed as a quartic function in two variables. Replacing $\lambda_{P,1}$ and $\lambda_{P,2}$ with x and y in (13), it gives

$$\begin{aligned} a_1x^4 + b_1xy^3 - c_1 = 0 \\ d_1x^3y + e_1y^4 - f_1 = 0 \end{aligned} \tag{22}$$

where

$$\begin{cases} a_1 = \sqrt{\frac{P_1}{r_{rx,1}}} \sum_{i=1}^{N_t} \frac{\omega^2 M_{i1}^2}{r_{tx,i}} \\ b_1 = \sqrt{\frac{P_2}{r_{rx,2}}} \sum_{i=1}^{N_t} \frac{\omega^2 M_{i1} M_{i2}}{r_{tx,i}} \\ c_1 = \sqrt{P_1 r_{rx,1}} \\ d_1 = \sqrt{\frac{P_1}{r_{rx,1}}} \sum_{i=1}^{N_t} \frac{\omega^2 M_{i1} M_{i2}}{r_{tx,i}} \\ e_1 = \sqrt{\frac{P_2}{r_{rx,2}}} \sum_{i=1}^{N_t} \frac{\omega^2 M_{i2}^2}{r_{tx,i}} \\ f_1 = \sqrt{P_2 r_{rx,2}}. \end{cases} \tag{23}$$

Sylvester matrix is used to get the solution of (22). Solving (24) directly and it will become an equation of degree 16 in one variable (25)

$$\begin{vmatrix} a_1 & 0 & 0 & b_1y^3 & -c_1 & 0 & 0 \\ 0 & a_1 & 0 & 0 & b_1y^3 & -c_1 & 0 \\ 0 & 0 & a_1 & 0 & 0 & b_1y^3 & -c_1 \\ d_1y & 0 & 0 & e_1y^4 - f_1 & 0 & 0 & 0 \\ 0 & d_1y & 0 & 0 & e_1y^4 - f_1 & 0 & 0 \\ 0 & 0 & d_1y & 0 & 0 & e_1y^4 - f_1 & 0 \\ 0 & 0 & 0 & d_1y & 0 & 0 & e_1y^4 - f_1 \end{vmatrix} = 0 \tag{24}$$

$$ay^{16} + by^{12} + cy^8 + dy^4 + e = 0 \tag{25}$$

where

$$\begin{cases} a = e_1(a_1e_1 - b_1d_1)^3 \\ b = f_1(b_1d_1 - 4a_1e_1)(b_1d_1 - a_1e_1)^2 \\ c = 3a_1{f_1}^2(2a_1e_1 - b_1d_1)(a_1e_1 - b_1d_1) \\ d = 3a_1{f_1}^2(2a_1e_1 - b_1d_1)(a_1e_1 - b_1d_1) \\ e = 3{a_1}^2b_1d_1{f_1}^3 - 4{a_1}^3e_1{f_1}^3 - {c_1}^3{d_1}^4 \\ f = {a_1}^3{f_1}^4. \end{cases} \tag{26}$$

Actually, (25) can be viewed as a quartic equation, and rooting finding formula exists in this case. Assuming

$$\begin{cases} \Delta_1 = c^2 - 3bd + 12ae \\ \Delta_2 = 2c^3 - 9bcd + 27ad^2 + 27b^2e - 72ace \\ \Delta = \frac{\sqrt[3]{2}\Delta_1}{3a\sqrt[3]{\frac{\Delta_2 + \sqrt{-4\Delta_1^3 + \Delta_2^2}}{2}}} + \frac{\sqrt[3]{\frac{\Delta_2 + \sqrt{-4\Delta_1^3 + \Delta_2^2}}{2}}}{3\sqrt[3]{2}a} \\ \Delta_3 = \frac{b^2}{4a^2} - \frac{2c}{3a} \\ \Delta_4 = -\frac{b^3}{a^3} + \frac{4bc}{a^2} - \frac{8d}{a} \end{cases} . \tag{27}$$

The solutions are

$$\begin{cases} y_1 = \left(\frac{-b}{4a} - \frac{1}{2}\sqrt{\Delta_3 + \Delta} - \frac{1}{2}\sqrt{2\Delta_3 - \Delta - \frac{\Delta_4}{\sqrt{2\Delta_3 + \Delta}}}\right)^{\frac{1}{4}} \\ y_2 = \left(\frac{-b}{4a} - \frac{1}{2}\sqrt{\Delta_3 + \Delta} + \frac{1}{2}\sqrt{2\Delta_3 - \Delta - \frac{\Delta_4}{\sqrt{2\Delta_3 + \Delta}}}\right)^{\frac{1}{4}} \\ y_3 = \left(\frac{-b}{4a} + \frac{1}{2}\sqrt{\Delta_3 + \Delta} - \frac{1}{2}\sqrt{2\Delta_3 - \Delta + \frac{\Delta_4}{\sqrt{2\Delta_3 + \Delta}}}\right)^{\frac{1}{4}} \\ y_4 = \left(\frac{-b}{4a} + \frac{1}{2}\sqrt{\Delta_3 + \Delta} + \frac{1}{2}\sqrt{2\Delta_3 - \Delta + \frac{\Delta_4}{\sqrt{2\Delta_3 + \Delta}}}\right)^{\frac{1}{4}} \end{cases} . \tag{28}$$

Although the derivation above is complicated, and the physical meaning is not clear. It means for a general two-RX system, the analytical solution still exists and can be solved without using numerical methods. However, for Case D2 ($N_t > 1, N_r > 2$), the analytical solution does not exist. It is the first time that the general ac analysis is explored to find the theoretical boundary of the optimal solution.

REFERENCES

[1] A. Ahmad, M. S. Alam, and A. A. S. Mohamed, "Design and interoperability analysis of quadruple pad structure for electric vehicle wireless charging application," *IEEE Trans. Transp. Electrific.*, vol. 5, no. 4, pp. 934–945, Dec. 2019.

[2] T. Yilmaz, N. Hasan, R. Zane, and Z. Pantic, "Multi-objective optimization of circular magnetic couplers for wireless power transfer applications," *IEEE Trans. Magn.*, vol. 53, no. 8, pp. 1–12, Aug. 2017.

[3] S. Bandyopadhyay, P. Venugopal, J. Dong, and P. Bauer, "Comparison of magnetic couplers for IPT-based EV charging using multi-objective optimization," *IEEE Trans. Veh. Technol.*, vol. 68, no. 6, pp. 5416–5429, Jun. 2019.

[4] S. Kim, G. A. Covic, and J. T. Boys, "Comparison of tripolar and circular pads for IPT charging systems," *IEEE Trans. Power Electron.*, vol. 33, no. 7, pp. 6093–6103, Jul. 2018.

[5] J. Deng, Y. Zhang, S. Wang, Z. Wang, and Y. Yang, "The design and coupler optimization of a single-transmitter coupled multireceiver inductive power transfer system for maglev trains," *IEEE Trans. Transp. Electrific.*, vol. 7, no. 4, pp. 3173–3184, Dec. 2021.

[6] E. Ayaz, O. Altun, H. Polat, and O. Keysan, "Fault tolerant multi-TX/multi-RX inductive power transfer system with a resonator coil," *IEEE J. Emerg. Sel. Topics Power Electron.*, vol. 11, no. 1, pp. 1272–1284, Feb. 2023.

[7] R. He, P. Zhao, M. Fu, Y. Liu, H. Wang, and J. Liang, "Decomposition and synthesis of high-order compensated inductive power transfer systems for improved output controllability," *IEEE Trans. Microw. Theory Techn.*, vol. 67, no. 11, pp. 4514–4523, Nov. 2019.

[8] W. Chen, W. Lu, H. H.-C. Iu, and T. Fernando, "Compensation network optimal design based on evolutionary algorithm for inductive power transfer system," *IEEE Trans. Circuits Syst. I: Reg. Papers*, vol. 67, no. 12, pp. 5664–5674, Dec. 2020.

[9] K. Zhao, G. Ning, R. He, H. Yang, H. Wang, and M. Fu, "An unsymmetrical driving scheme for inductive power transfer systems using decoupled transmitter coils," *IEEE J. Emerg. Sel. Topics Ind. Electron.*, vol. 4, no. 2, pp. 614–624, Apr. 2023.

[10] Z. Zhang, X. Li, H. Pang, H. Komurcugil, Z. Liang, and R. Kennel, "Multiple-frequency resonating compensation for multichannel transmission of wireless power transfer," *IEEE Trans. Power Electron.*, vol. 36, no. 5, pp. 5169–5180, May 2021.

[11] Y. Huang, C. Liu, Y. Xiao, and S. Liu, "Separate power allocation and control method based on multiple power channels for wireless power transfer," *IEEE Trans. Power Electron.*, vol. 35, no. 9, pp. 9046–9056, Sep. 2020.

[12] H. Pang, K. T. Chau, W. Liu, and X. Tian, "Multi-resonating-compensation for multi-channel multi-pickup wireless power transfer," *IEEE Trans. Magn.*, vol. 58, no. 8, pp. 1–6, Aug. 2022.

[13] T. Diekhans and R. W. De Doncker, "A dual-side controlled inductive power transfer system optimized for large coupling factor variations and partial load," *IEEE Trans. Power Electron.*, vol. 30, no. 11, pp. 6320–6328, Nov. 2015.

[14] W. X. Zhong and S. Y. R. Hui, "Maximum energy efficiency tracking for wireless power transfer systems," *IEEE Trans. Power Electron.*, vol. 30, no. 7, pp. 4025–4034, Jul. 2015.
[15] Z. Huang, S.-C. Wong, and C. K. Tse, "Control design for optimizing efficiency in inductive power transfer systems," *IEEE Trans. Power Electron.*, vol. 33, no. 5, pp. 4523–4534, May 2018.
[16] Z. Zhang, H. Pang, S. H. K. Eder, and R. Kennel, "Self-balancing virtual impedance for multiple-pickup wireless power transfer," *IEEE Trans. Power Electron.*, vol. 36, no. 1, pp. 958–967, Jan. 2021.
[17] J.-W. Kim, I.-J. Hwang, J.-W. Yu, and T.-D. Yeo, "Maximum efficiency point tracking scheme for loosely coupled multiple-receiver wireless power charging system with mutual inductance tracking," *IEEE Trans. Microw. Theory Techn.*, vol. 69, no. 1, pp. 378–386, Jan. 2021.
[18] J. Xu, X. Li, H. Li, Z. Xie, and Q. Ma, "Maximum efficiency tracking for multitransmitter multireceiver wireless power transfer system on the submerged buoy," *IEEE Trans. Ind. Electron.*, vol. 69, no. 2, pp. 1909–1919, Feb. 2022.
[19] Y. Liu, C. Liu, Z. Dong, S. Liu, and W. Wang, "A novel wireless energy router for home energy management with omnidirectional power transmission," *IEEE Trans. Ind. Electron.*, vol. 70, no. 9, pp. 8979–8990, Sep. 2023.
[20] M. Fu, H. Yin, X. Zhu, and C. Ma, "Analysis and tracking of optimal load in wireless power transfer systems," *IEEE Trans. Power Electron.*, vol. 30, no. 7, pp. 3952–3963, Jul. 2015.
[21] R. He, P. Zhao, G. Ning, K. Yue, Y. Liu, and M. Fu, "Optimal driving and loading scheme for multiple-receiver inductive power transfer," *IEEE Trans. Ind. Electron.*, vol. 69, no. 12, pp. 12665–12675, Dec. 2022.
[22] D.-H. Kim and D. Ahn, "Maximum efficiency point tracking for multiple-transmitter wireless power transfer," *IEEE Trans. Power Electron.*, vol. 35, no. 11, pp. 11391–11400, Nov. 2020.
[23] Z. Yan et al., "Efficiency improvement of wireless power transfer based on multitransmitter system," *IEEE Trans. Power Electron.*, vol. 35, no. 9, pp. 9011–9023, Sep. 2020.
[24] M. Fu, T. Zhang, C. Ma, and X. Zhu, "Efficiency and optimal loads analysis for multiple-receiver wireless power transfer systems," *IEEE Trans. Microw. Theory Techn.*, vol. 63, no. 3, pp. 801–812, Mar. 2015.
[25] D. Ahn, S.-M. Kim, S.-W. Kim, J.-I. Moon, and I.-K. Cho, "Wireless power transfer receiver with adjustable coil output voltage for multiple receivers application," *IEEE Trans. Ind. Electron.*, vol. 66, no. 5, pp. 4003–4012, May 2019.
[26] Q.-T. Duong and M. Okada, "Maximum efficiency formulation for multiple-input multiple-output inductive power transfer systems," *IEEE Trans. Microw. Theory Techn.*, vol. 66, no. 7, pp. 3463–3477, Jul. 2018.
[27] A. Hossain, P. Darvish, S. Mekhilef, K. S. Tey, and C. W. Tong, "A new coil structure of dual transmitters and dual receivers with integrated decoupling coils for increasing power transfer and misalignment tolerance of wireless EV charging system," *IEEE Trans. Ind. Electron.*, vol. 69, no. 8, pp. 7869–7878, Aug. 2022.
[28] R. Fletcher, *Practical Methods of Optim.* New York, NY, USA: Wiley, 2000. [Online]. Available: https://books.google.at/books?id=z3m_EAAAQBAJ
[29] A. Zaheer, G. A. Covic, and D. Kacprzak, "A bipolar pad in a 10-kHz 300-W distributed IPT system for AGV applications," *IEEE Trans. Ind. Electron.*, vol. 61, no. 7, pp. 3288–3301, Jul. 2014.
[30] S. Kim, G. A. Covic, and J. T. Boys, "Tripolar pad for inductive power transfer systems for EV charging," *IEEE Trans. Power Electron.*, vol. 32, no. 7, pp. 5045–5057, Jul. 2017.
[31] E. S. Lee, J. S. Choi, H. S. Son, S. H. Han, and C. T. Rim, "Six degrees of freedom wide-range ubiquitous IPT for IoT by DQ magnetic field," *IEEE Trans. Power Electron.*, vol. 32, no. 11, pp. 8258–8276, Nov. 2017.
[32] J. Feng, Q. Li, F. C. Lee, and M. Fu, "Transmitter coils design for free-positioning omnidirectional wireless power transfer system," *IEEE Trans. Ind. Informat.*, vol. 15, no. 8, pp. 4656–4664, Aug. 2019.
[33] J. J. Casanova, Z. N. Low, and J. Lin, "A loosely coupled planar wireless power system for multiple receivers," *IEEE Trans. Ind. Electron.*, vol. 56, no. 8, pp. 3060–3068, Aug. 2009.
[34] W. Chen, H. Li, and W. Lu, "Decoupling design of multi-coil wireless power transfer system with metal insulator," in *Proc. IEEE PELS Workshop Emerg. Technol.: Wirel. Power Transfer*, 2017, pp. 30–33.
[35] W. Chen, K. Ji, Y. Zhang, and J. Wang, "Design and analysis of multiload inductive power transfer system using bilateral-excitation scheme," *IEEE Trans. Ind. Informat.*, vol. 18, no. 1, pp. 365–374, Jan. 2022.

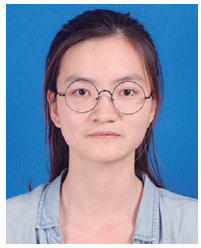

Rong He (Member, IEEE) received the B.S degree in electrical engineering and automation from the Harbin Institute of Technology, Weihai, China, in 2018. She is currently working toward the Ph.D. degree in power electronics with the School of Information Science and Technology, ShanghaiTech University, Shanghai, China.

Her research interests include the compensation of the IPT system and multiple-coil IPT systems.

Xinlin Wang (Graduate Student Member, IEEE) received the B.S. degree in electrical engineering and automation from the Hohai University, Nanjing, China, 2020. He is currently working toward the master's degree in power electronics with the School of Information Science and Technology, ShanghaiTech University, Shanghai, China.

His research interests include multiple-coil IPT systems and bidirectional IPT systems.

Haoyu Wang (Senior Member, IEEE) received the Bachelor's degree (with Distinguished Hons.) in electrical engineering from Zhejiang University, Hangzhou, China, in 2009, and the Ph.D. degree in electrical engineering from the University of Maryland, College Park, MD, USA, in 2014.

In 2014, he joined the School of Information Science and Technology, ShanghaiTech University, Shanghai, China, where he is currently a tenured Associate Professor. His research interests include power electronics, plug-in electric and hybrid electric vehicles, and the applications of wide-bandgap semiconductors.

Dr. Wang is an Associate Editor for IEEE TRANSACTIONS ON INDUSTRIAL ELECTRONICS, IEEE TRANSACTIONS ON TRANSPORTATION ELECTRIFICATION, and *CPSS Transactions on Power Electronics and Applications*.

Minfan Fu (Senior Member, IEEE) received the B.S., M.S., and Ph.D. degrees in electrical and computer engineering from the Shanghai Jiao Tong University, Shanghai, China, in 2010, 2013, and 2016, respectively.

From 2016 to 2018, he held a Postdoctoral position with the Center for Power Electronics Systems, Virginia Polytechnic Institute and State University, Blacksburg, VA, USA. He is currently an Assistant Professor with the School of Information Science and Technology, ShanghaiTech University, Shanghai. He has authored or coauthored more than 100 papers in IEEE journals and conferences. His research interests include wireless power transfer, high-frequency power conversion, and application of wide-bandgap devices.